Free Radical Biology and Medicine 73 (2014) 154–165

Contents lists available at ScienceDirect

Free Radical Biology and Medicine

journal homepage: www.elsevier.com/locate/freeradbiomed

Original Contribution

ESR evidence for in vivo formation of free radicals in tissue of mice exposed to single-walled carbon nanotubes

A.A. Shvedova [a,b,*], E.R. Kisin [a], A.R. Murray [a,b], A. Mouithys-Mickalad [c], K. Stadler [d], R.P. Mason [d], M. Kadiiska [d]

[a] Pathology and Physiology Research Branch, HELD, National Institute for Occupational Safety and Health, Morgantown, WV 26505, USA
[b] Physiology and Pharmacology, West Virginia University, Morgantown, WV 26506, USA
[c] University of Liege, Liège 4000, Belgium
[d] National Institute of Environmental Health Science, Research Triangle Park, NC 27709, USA

ARTICLE INFO

Article history:
Received 2 January 2014
Received in revised form
28 April 2014
Accepted 16 May 2014
Available online 23 May 2014

Keywords:
Free radicals
Carbon nanotubes
in vivo
Tissues
Oxidative stress
Inflammation

ABSTRACT

Nanomaterials are being utilized in an increasing variety of manufactured goods. Because of their unique physicochemical, electrical, mechanical, and thermal properties, single-walled carbon nanotubes (SWCNTs) have found numerous applications in the electronics, aerospace, chemical, polymer, and pharmaceutical industries. Previously, we have reported that pharyngeal exposure of C57BL/6 mice to SWCNTs caused dose-dependent formation of granulomatous bronchial interstitial pneumonia, fibrosis, oxidative stress, acute inflammatory/cytokine responses, and a decrease in pulmonary function. In the current study, we used electron spin resonance (ESR) to directly assess whether exposure to respirable SWCNTs caused formation of free radicals in the lungs and in two distant organs, the heart and liver. Here we report that exposure to partially purified SWCNTs (HiPco technique, Carbon Nanotechnologies, Inc., Houston, TX, USA) resulted in the augmentation of oxidative stress as evidenced by ESR detection of α-(4-pyridyl-1-oxide)-*N*-*tert*-butylnitrone spin-trapped carbon-centered lipid-derived radicals recorded shortly after the treatment. This was accompanied by a significant depletion of antioxidants and elevated biomarkers of inflammation presented by recruitment of inflammatory cells and an increase in proinflammatory cytokines in the lungs, as well as development of multifocal granulomatous pneumonia, interstitial fibrosis, and suppressed pulmonary function. Moreover, pulmonary exposure to SWCNTs also caused the formation of carbon-centered lipid-derived radicals in the heart and liver at later time points (day 7 postexposure). Additionally, SWCNTs induced a significant accumulation of oxidatively modified proteins, increase in lipid peroxidation products, depletion of antioxidants, and inflammatory response in both the heart and the liver. Furthermore, the iron chelator deferoxamine noticeably reduced lung inflammation and oxidative stress, indicating an important role for metal-catalyzed species in lung injury caused by SWCNTs. Overall, we provide direct evidence that lipid-derived free radicals are a critical contributor to tissue damage induced by SWCNTs not only in the lungs, but also in distant organs.

Published by Elsevier Inc.

Single-walled carbon nanotubes (SWCNTs) are an allotrope of carbon formed by a sheet of graphene rolled into a seamless cylinder with a diameter of 1–4 nm and a length ranging from 100 nm to 1.5 μm. SWCNTs exhibit unique electronic and mechanical properties that are used in numerous applications such as field-emission displays, nanocomposites, nanosensors, conductive plastics, paints, technical textiles and repelling features for garments, and biomedical applications. These materials are also on the leading edge of electronic fabrication and are expected to play a major role in the next generation of miniaturized electronics and in energy storage, such as hydrogen fuel cells and other efficient renewable energy sources [1–6]. However, knowledge of the potential health and environmental risks that may occur throughout the entire life cycle of products is limited [5,7].

The intrinsic toxicity of SWCNTs has been attributed to their distinctive physicochemical properties, including their small particle size and the large surface area of the carbon tube decorated with catalytic transition metals (iron, cobalt, nickel, etc.) that are known to trigger generation of free radicals and oxidative stress. Oxidative stress is one of the well-known mechanisms of SWCNT-induced toxicity [8,9]. It is believed that free radical formation by

* Corresponding author at: NIOSH, Pathology and Physiology Research Branch, Health Effects Laboratory Division, 1095 Willowdale Road, Morgantown, WV 26505, United States. Fax: +304 285 5938.
E-mail address: ats1@cdc.gov (A.A. Shvedova).

http://dx.doi.org/10.1016/j.freeradbiomed.2014.05.010
0891-5849/Published by Elsevier Inc.

SWCNTs is realized via several mechanisms, frequently involving redox-cycling pathways.

There are many reports showing in vitro generation of free radicals in a number of mammalian cell types exposed to SWCNTs by employing various intracellular fluorescent dyes [10–12]. Fluorescent dye probes provide convenient, fast, and easy methods to detect oxidative stress in cells [13]. Usually these compounds are nonfluorescent (or weakly fluorescent), but yield highly fluorescent products upon reaction with free radicals. However, a major concern is the generation (or photogeneration) of free radicals by the probes themselves and/or their reaction products, which may result in artifactual results and/or higher backgrounds [14,15].

The oxidative modification of biomolecules has been systematically observed under normal and pathological conditions [16,17]. However, to understand the role of redox chemistry in the observed health outcomes and its role in the development of disease, many steps during the generation of free radicals must be linked: the identification of the biomolecule(s) that is the target of oxidative modification, the specific residue(s) at which the radicals are formed, metabolic activation targeting cellular/subcellular structures and tissue injury, and ultimately the whole-body inflammatory responses. The only tool that directly provides evidence of free radical formation is the electron spin resonance (ESR) spin trapping technique, which currently is the "gold standard" for the measurement of free radicals [16]. Previously, we and others reported employing nitrone spin trapping agents, e.g., α-(4-pyridyl-1-oxide)-*N*-*tert*-butylnitrone (POBN), to detect free radical species in tissues and organs of animals exposed to either chemicals [8,18–20] or airborne particulates [21,22]. The use of POBN spin trapping is a critical technical approach to identifying radical adducts (lipid and/or protein radical adducts) by extending short radical lifetimes and enabling timely recording of free radicals in many biological systems in vitro and in vivo, including tissue samples and biological fluids from living organisms.

In addition to possible direct effects of carbon nanotubes (CNTs) in the lung after inhalation/aspiration exposure, carbon nanomaterials have been shown to translocate to secondary target organs [23,24]. Pulmonary exposure to CNTs has been shown to cause dose-dependent inflammation and necrosis within the liver and kidney, reductions in the serum antioxidant capacity, indirect thrombogenic effects within the liver and heart, microvascular dysfunction, and possible effects on cardiac autonomic regulation [24–30]. Mercer and colleagues [31] demonstrated that multi-walled carbon nanotubes (MWCNTs) deposited in the lungs were transported to the pleura, respiratory musculature, liver, kidney, heart, and brain. Matthews et al. [32] examined and predicted cumulative pulmonary translocation of SWCNTs from the lung airways of rats using an ex vivo isolated perfused-lung model.

Here for the first time we provide evidence for in vivo generation of carbon-centered free radicals in mouse lungs, heart, and liver after exposure to respirable SWCNTs. We demonstrate that the carbon-centered lipid-derived radicals detected are an intermediate of enhanced lipid peroxidation in the lung, then later in the heart and liver, in response to SWCNTs. Pulmonary exposure to SWCNTs induced oxidative stress and significantly reduced the level of antioxidants in mouse lungs, facilitating recruitment of inflammatory cells and increasing the profile of proinflammatory cytokines in the bronchoalveolar lavage (BAL) fluids. However, at a later time point (7 days postexposure), SWCNTs triggered a significant accumulation of oxidatively modified protein carbonyls, an increase in lipid peroxidation products, a decrease in protein thiols, the depletion of glutathione (GSH), and signs of inflammation only in the heart and liver. Additionally, the metal chelator deferoxamine (DFO) significantly inhibited biomarkers of inflammation and oxidative stress in the lung, demonstrating an important role for metal-catalyzed species in lung injury caused by SWCNTs.

Methods

Animals and treatments

Specific-pathogen-free adult female C57BL/6 mice (7–8 weeks of age) were supplied by The Jackson Laboratory (Bar Harbor, ME. USA) and weighed 20.3 ± 0.21 g at the time of use. Animals were individually housed in AAALAC-approved NIOSH animal facilities in microisolator cages for 1 week before use. Autoclaved Beta Chip bedding (Northeastern Products Corp., Warrensburg, NY, USA) was changed weekly. Animals were supplied with water and Harlan Teklad, 7913, NIH-31 Modified Mouse/Rat Diet, Irradiated (Harlan Teklad, Madison, WI, USA) and housed under controlled light, temperature, and humidity conditions. Experiments were conducted under a protocol approved by the Animal Care and Use Committee of the National Institute for Occupational Safety and Health.

A suspension of SWCNTs (40–80 μg/mouse) was used for a single pharyngeal aspiration of C57BL/6 mice, whereas the corresponding control mice were administered a sterile $Ca^{2+}+Mg^{2+}$-free phosphate-buffered saline (PBS) vehicle. Mice were sacrificed on days 1 and 7 after exposure. For each group, six animals were used to evaluate BAL (cell differential and cytokine accumulation), fibrogenic responses, tissue damage, inflammation, and oxidative stress markers and to conduct histopathology. To study free radical generation, POBN (6 mmol/kg) was injected intraperitoneally (ip) 30 min before tissue collection. To investigate whether hydroxyl radicals were produced in the lungs of SWCNT-treated mice, the ^{13}C-labeled dimethyl sulfoxide ([^{13}C]DMSO, 1 ml/kg) was administered together with POBN to another group of mice. Lipid extracts of the lungs, liver, and heart were used to measure radical adduct content. An additional group of mice was pretreated with DFO (100 mg/kg, ip, 2 and 24 h before pharyngeal aspiration of SWCNTs). Inflammation and oxidative stress markers were measured in the lung homogenates of mice sacrificed 24 h after exposure to SWCNTs.

Particles

The SWCNTs (Carbon Nanotechnologies, Inc., Houston, TX, USA) used in this study were produced by the high-pressure CO disproportionation process (HiPco) technique [33], employing CO in a continuous-flow gas phase as the carbon feedstock and Fe $(CO)_5$ as the iron-containing catalyst precursor, and purified by acid treatment to remove metal contaminants [34]. The particles were characterized by chemical analysis using the NIOSH *Manual of Analytical Methods* No. 5040 and inductively coupled plasma atomic emission spectroscopy. SWCNTs were 99.7% wt elemental carbon with 0.23% wt iron. Individual SWCNTs had diameters ranging from 1 to 4 nm and were 1–3 μm in length. SWCNTs were found to have a specific surface area of 1040 m^2/g. Detailed particle characterization was published in [44]. Before animal exposure, particles were ultrasonicated (30 s × 3 cycles) on ice for improved dispersion of nanoparticles using a Vibra Cell (Sonics and Materials, Newtown, CT, USA) probe sonicator operating at 20 kHz (6.5% power).

Particulate instillation

Mouse pharyngeal aspiration was used for particulate administration. Briefly, after anesthetization with a mixture of ketamine (Phoenix, St. Joseph, MO, USA) and xylazine (Phoenix) (62.5 and 2.5 mg/kg subcutaneously in the abdominal area), the mouse was placed on a board in a near-vertical position and the animal's tongue extended with lined forceps. A suspension (approximately 50 μl) of particulates prepared in PBS with SWCNTs at a dose of 0,

40, or 80 μg/mouse was placed in the posterior of the throat and the tongue held until the suspension was aspirated into the lungs. All particles were sterilized before administration. Control mice were administered a sterile $Ca^{2+}+Mg^{2+}$-free PBS vehicle. All mice in the particle and PBS groups survived the exposure procedure.

Obtaining bronchoalveolar lavage from mice

Mice were weighed and euthanized with an intraperitoneal injection of sodium pentobarbital (Fort Dodge Animal Health, Fort Dodge, IA. USA) (> 100 mg/kg). The trachea was cannulated with a blunted 22-gauge needle, and BAL was performed using cold sterile $Ca^{2+}+Mg^{2+}$-free PBS at a volume of 0.9 ml for the first lavage (kept separate) and 1.0 ml for subsequent lavages. Approximately 5 ml of BAL fluid per mouse was collected and pooled in sterile centrifuge tubes. Pooled BAL cells were washed in $Ca^{2+}+Mg^{2+}$-free PBS by alternate centrifugation (800*g* for 10 min at 4 °C) and resuspended. Cell-free first-fraction BAL aliquots were frozen or kept until processed.

BAL cell counting and differentials

The degree of inflammatory response induced by the pharyngeal aspirated particulates was estimated by counting the total number of cells, macrophages, and neutrophils recruited into the mouse lungs and recovered in the BAL fluid. Cell counts were performed using an electronic cell counter equipped with a cell sizing attachment (Coulter Model Multisizer II with a 256C channelizer; Coulter Electronics, Hialeah, FL, USA). Alveolar macrophages, polymorphonuclear leukocytes, and lymphocytes were identified by their characteristic cell shapes in centrifuge smears stained with a Hema-3 kit (Fisher Scientific, Pittsburgh, PA, USA), and differential counts of BAL cells were carried out. Three hundred cells per slide were counted.

Cytokine analysis

Cytokines, tumor necrosis factor (TNF-α) and interleukin-6 (IL-6), in the acellular BAL fluid from mice exposed to SWCNTs were assayed using a BD Cytometric Bead Array, Mouse Inflammation kit (BD Biosciences, San Diego, CA, USA). Additionally, the level of transforming growth factor β (TGF-β1) in the BAL was determined using an ELISA kit (Biosource International, Camarillo, CA, USA). Proinflammatory cytokines, IL-1α, IL-6, interferon-γ (IFN-γ), and TNF-α, in the lung homogenates from mice exposed to SWCNT were analyzed using a Bio-Plex system (Bio-Rad Laboratories, Hercules, CA, USA). The 40-fold-diluted aliquots of lung homogenates (50 μl taken as is) in each case were used for analyzing and estimating the concentrations of cytokines. The concentrations were calculated using Bio-Plex Manager 6.1 software (Bio-Rad) based on standard curves.

Total protein and lactate dehydrogenase (LDH) activity in BAL fluid

The level of pulmonary injury was ascertained by evaluating the levels of protein and LDH in the acellular BAL fluid obtained from the mice on day 1 after exposure to SWCNTs. Total protein in the BAL supernatant was measured with a modified Bradford assay according to the manufacturer's instructions (Bio-Rad) with bovine serum albumin as a standard. The activity of LDH in unfrozen BAL samples was assayed spectrophotometrically by monitoring the reduction of nicotinamide adenine dinucleotide at 340 nm in the presence of lactate (Pointe Scientific, Inc., Lincoln Park, MI, USA).

in vivo ESR studies

The technique of spin trapping involves the indirect detection of primary free radicals that cannot be directly observed by conventional ESR owing to low steady-state concentrations and/or very short relaxation times, which lead to very broad lines [35]. We used organic extraction to concentrate the spin-trapped radicals. It is known that the limitation of organic extraction is that only nonpolar radical adducts that are soluble in chloroform, such as the POBN lipid-derived radicals, can be detected. In addition, the radical adduct must be stable enough to survive not only the biological environment in which it was formed but also homogenization of the tissue and the time required for solvent extraction and evaporation. We chose POBN as our spin trap because it readily traps lipid radicals, and the adducts are stable in lipid extraction of tissue for the requisite time.

C57BL/6 mice were exposed by pharyngeal aspiration to partially purified SWCNTs (40 μg/mouse). POBN (6 mmol/kg) was injected (ip) 30 min before tissue collection. Tissue samples (lung, heart, liver) were minced and homogenized in 2.5 ml of 2:1 chloroform:methanol, 0.5 ml of 30 mM 2,2′-dipyridyl, 2 ml of 1.2 mM ultrapure phenol, and 2 ml of deionized water using a homogenizer (Fisher Scientific Power Gen 125) in an ice bath. The 2,2′-dipyridyl was used to inhibit ex vivo ferrous-dependent reactions. The phenol was used as an antioxidant to protect from ex vivo oxidation. To the homogenate obtained above, 16 ml of 2:1 chloroform:methanol was added, and the resulting sample was shaken and then centrifuged at 2000 rpm for 10 min (Beckman, TJ-6) as describrd previously [21,36]. The chloroform layer was isolated and dried by passing through a sodium sulfate column. The solvent was evaporated to 1.0 ml of solution by bubbling with N_2.

Immediately after solvent evaporation, ESR spectra were recorded at room temperature using a quartz flat cell in a Bruker EMX EPR spectrometer equipped with a Super High Q cavity. Spectra were recorded on an IBM-compatible computer interfaced with the spectrometer with instrument settings of 9.79 GHz, 20.2 mW microwave power, 100 kHz modulation frequency, 1300 ms conversion time, and a 655 ms time constant. The ESR spectra were simulated with a computer optimization procedure as described by Duling [37].

Preparation of lung homogenates

The whole mouse lungs, hearts, and livers were separated from other tissues and weighed before being homogenized with a tissue tearer (Model 985-370, Biospec Products, Inc., Racine, WI, USA) in PBS (pH 7.4) for 2 min. The homogenate suspensions were aliquotted and frozen at −80 °C until processed.

Tissue injury and inflammation markers

Tissue damage was evaluated by measuring the level of LDH in the lungs, heart, and liver 7 days after exposure to SWCNTs. LDH activity in the tissue homogenates was assayed spectrophotometrically by monitoring the reduction of nicotinamide adenine dinucleotide at 340 nm in the presence of lactate (Pointe Scientific). Inflammation response in the lungs, heart, and liver of mice was assessed by measurement of myeloperoxidase (MPO) activity in tissue homogenates using a commercially available ELISA colorimetric assay (Northwest Life Science Specialties, Vancouver, WA, USA). Results for both LDH and MPO activity were normalized to total protein content in tissue homogenate samples.

Fluorescence assay of GSH and protein sulfhydryls in the tissue homogenates

Total thiol concentration in the lung, heart, or liver homogenates was determined using ThioGlo-1, a maleimide reagent that produces a highly fluorescent product upon its reaction with SH groups [10]. A standard curve was established by addition of GSH (0.04–2.0 mM) to 0.1 M phosphate buffer (pH 7.4) containing 10 μM ThioGlo-1. GSH content was estimated by an immediate fluorescent response registered upon addition of ThioGlo-1 to a tissue homogenate. Total protein sulfhydryls were determined from the additional fluorescent response after addition of sodium dodecyl sulfate (4 mM) to the same homogenate. A CytoFluor Multiwell Plate Reader Series 4000 (Applied Biosystems, Foster City, CA, USA) was employed for the assay of fluorescence using excitation at 360/40 nm and emission at 530/25 nm with a gain of 50. The data obtained were exported and analyzed using CytoFluor software (Applied Biosystems).

Evaluation of biomarkers of oxidative stress in the BAL fluids and tissue homogenates

Oxidative damage to the lungs, heart, and liver after pulmonary exposure to SWCNTs was evaluated by the presence of hydroxynonenal–histidine (HNE–His) protein adducts and protein carbonyl formation. HNE has been shown to be capable of binding to proteins and forming stable adducts, also termed advanced lipid peroxidation end products. HNE–His adducts were measured in BAL fluids (day 1) or tissue homogenates (days 1 and 7) by ELISA using an OxiSelect HNE–His adduct kit (Cell Biolabs, Inc., San Diego, CA, USA). The quantity of HNE–His adducts in protein samples was determined by comparing its absorbance with that of a known HNE–bovine serum albumin standard curve. The quantity of oxidatively modified proteins as assessed by measurement of protein carbonyls in tissue homogenates was determined using a Biocell PC ELISA kit (Northwest Life Science Specialties). Sensitivity of the assay was <0.1 nmol/mg protein.

Lung fixation and histopathology

Lung tissues were prepared for histological analysis using standard conditions. Animals were deeply anesthetized with an overdose of sodium pentobarbital. The trachea was exposed, cannulated, and secured with a suture. Before instillation of the fixative, the diaphragm was ruptured to collapse the lungs. The lungs were subsequently fixed with 1% paraformaldehyde/0.1% glutaraldehyde in situ at 5 cm of pressure for 0.2 h. Thereafter, the trachea was ligated and the lungs were excised and submerged in fixative overnight before embedding. Lung tissue slices were prepared from both right and left lung lobes and embedded in paraffin. Sections (5 μm) were prepared using an HM 320 rotary microtome (Carl Zeiss, Thornwood, NY, USA). Lung specimens were stained with hematoxylin and eosin (H&E). Airways, terminal bronchioles, and the lung parenchyma were examined microscopically for the presence of cellular changes and inflammation.

Lung collagen measurements

Total lung collagen content was determined by quantifying total soluble collagen using a Sircol collagen assay kit (Accurate Chemical and Scientific Corp., Westbury, NY, USA). Briefly, whole lungs were homogenized in 0.7 ml of 0.5 M acetic acid containing pepsin (Accurate Chemical and Scientific Corp.) with a 1:10 ratio of pepsin:tissue (wet weight). Each sample was stirred vigorously for 24 h at 4 °C and centrifuged, and 200 μl of supernatant was assayed according to the manufacturer's instructions.

Measurement of pulmonary function

Spontaneous breathing patterns were monitored using whole-body plethysmography. Breathing patterns were monitored 24 h before SWCNT exposure (baseline) and then 1 and 7 days after exposure to detect treatment-related changes. Mice were acclimated to the plethysmograph for 10 min, followed by 10 min of acquisition of spontaneous breathing data. Expiratory time was calculated from the raw waveforms using Biosystem XA software (Buxco Electronics, Inc., Wilmington, NC, USA) and expressed as a percentage of baseline.

Protein assay

Measurements of protein in tissue homogenates from mouse lung, heart, and liver were run using a Bio-Rad protein assay kit (Cat. No. 500-0006).

Statistics

Data were expressed as the mean ± SEM for each group. A one-way ANOVA was employed to compare the responses between treatments. Statistical significance was set at $p<0.05$.

Results

Detection of free radicals in mouse lungs, liver, and heart after exposure to SWCNTs

A stable six-line ESR spectrum was reproducibly detected in the lung extract of POBN-injected mice 24 h after SWCNT administration (40 μg/mouse, Fig. 1A). Composite computer simulation of the spectra (Fig. 1B) allowed us to characterize and confirm the identity of the radical species being trapped as POBN–lipid radical adducts. The hyperfine coupling constants for the POBN radical adducts were $a^N=14.90\pm0.02$ G and $a^H_\beta=2.56\pm0.04$ G, similar to those previously reported for the POBN–radical adducts of carbon-centered, lipid-derived radicals [21,36,38–42]. Lipid extracts from control animals (Fig. 1C) showed only a negligible background signal. Without the spin trap, neither SWCNTs nor PBS aspiration yielded a detectable spectrum. The sixfold increase in signal intensity of the POBN radical adducts in SWCNT-treated lungs compared to PBS-treated lungs was statistically significant (Fig. 1D). To investigate whether hydroxyl radicals were produced in the lungs of SWCNT-treated mice, the hydroxyl radical scavenger DMSO was administered to mice because it is well known that a reaction between DMSO and hydroxyl radicals will yield $^{\bullet}CH_3$, which in the presence of O_2 is converted to $^{\bullet}OCH_3$ [40,43]. The $^{\bullet}CH_3$ and $^{\bullet}OCH_3$ are then detected as POBN adducts. The amount of POBN lipid radicals did not appear to increase in the presence of DMSO, and experiments with ^{13}C-labeled DMSO (1 mg/kg) did not change the appearance of the six-line ESR signal shown in Fig. 1. Either this approach failed to detect the hydroxyl radical or another species is responsible for the initiation of lipid peroxidation (Fig. 1A).

To determine the late effect of SWCNTs on free radical generation, we evaluated the ESR signal of POBN radical adducts in lipid extracts of mouse lungs, heart, and liver 7 days postexposure. Lipid extracts of heart and liver tissue acquired from mice exposed to SWCNTs demonstrated an ESR spectrum identical to the prominent six-line radical adduct spectra from lungs of those animals 24 h post-SWCNT exposure (Figs. 2B and D). The hyperfine coupling constants for the POBN–radical adducts were also not different from those determined for the lipid extract of lung tissue 24 h postexposure, i.e., $a^N=14.9$ G and $a^H_\beta=2.5$ G. Moreover, we

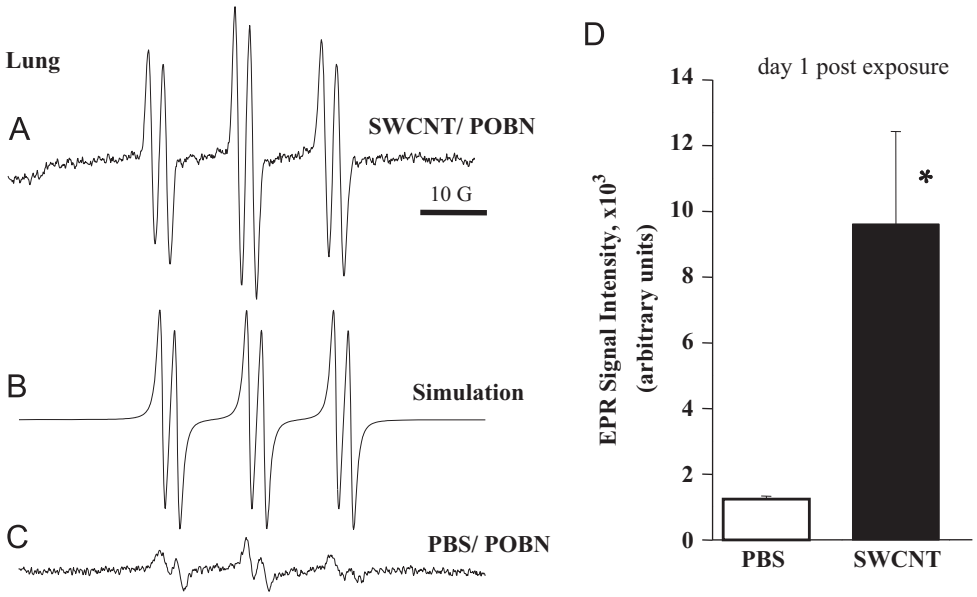

Fig. 1. Free radical generation in lipid extracts of lungs 24 h after treatment with SWCNTs. (A) Representative ESR spectrum of POBN radical adducts detected in lungs 30 min after injection of the spin trap POBN (6 mmol/kg, ip). (B) Computer simulation of the spectrum in (A). (C) Same as for (A) but mice were treated with PBS. (D) Results of relative values of ESR signal intensity (arbitrary units) represent the mean ± SE derived from four or five independent experiments. $*p < 0.001$, significantly different from controls. C57BL/6 mice were exposed by pharyngeal aspiration to partially purified SWCNTs (40 μg/mouse). POBN (6 mmol/kg) was injected (ip) 30 min before tissue collection. Instrumental settings of the Bruker ESR spectrometer were as follows: microwave power, 20 mW; modulation amplitude, 1 G; conversion time, 0.6 s; time constant, 1.3 s.

did not observe a significant increase in the signal intensity of the POBN–radical adduct in SWCNT-treated lungs compared to PBS-treated control samples; however, a significant increase in the generation of free radicals (1.67- and 2.65-fold versus PBS control groups) was detected in the lipid extracts of heart and liver tissues, respectively (Fig. 2E). The injection with PBS resulted only in an ESR background signal (Figs. 2A and C), confirming the dependence of radical formation on the SWCNT exposure.

Inflammatory response and tissue damage

To characterize tissue injury and inflammatory responses to SWCNTs, we compared the cell differential, total cell counts, cytokines, protein, LDH, and MPO levels in the BAL fluids or in tissue (lung, heart, liver) homogenates of C57BL/6 mice on days 1 and 7 postexposure.

BAL cytology indicated a robust accumulation of neutrophils after pharyngeal exposure to SWCNTs with a maximum on day 1 post-treatment (80-fold over control, Fig. 3A). No significant changes in alveolar macrophages (AMs) or total cells were detected on either day 1 or 7 postexposure.

The most significant induction of proinflammatory cytokines was observed in the BAL fluids of C57BL/6 mice 1 day post-pharyngeal aspiration of 40 μg/mouse SWCNTs (Fig. 3B). At this time point, levels of TNF-α and IL-6 were 22.5- and 11.9-fold higher than in the PBS control groups, respectively. No significant changes in BAL proinflammatory cytokines were detected on day 7 postexposure.

Changes in lung permeability were assessed by the level of protein in the BAL fluid. Pharyngeal aspiration of SWCNTs significantly increased BAL protein by 3.8-fold over the respective controls on day 1 postexposure (Fig. 3C). The degree of pulmonary damage caused by SWCNT pharyngeal aspiration was assessed by LDH enzyme activity in the BAL fluid recovered from the mice. The level of LDH response after SWCNT (40 μg/mouse) aspiration observed on day 1 was significantly increased (1.8-fold) over the control (Fig. 3C).

The degree of tissue injury caused by SWCNTs (40–80 μg/mouse) on day 7 post-pharyngeal aspiration was assessed by LDH activity in the lung, heart, and liver homogenates (Fig. 4A). The cytotoxicity response after SWCNT aspiration (~25% increase over control) was observed at both concentrations (40 and 80 μg/mouse). Measurements of dose-dependent LDH accumulation revealed significant 10 and 24% increases over the control groups in liver homogenates from mice exposed to 40 and 80 μg/mouse of SWCNTs, respectively. The levels of LDH in the heart homogenates were increased by 22% only at the highest concentration of SWCNTs.

The degree of tissue inflammation caused by SWCNTs on day 7 post-pharyngeal aspiration was assessed by the level of MPO activity in the lung, heart, and liver homogenates (Fig. 4B). The tissue inflammation response after SWCNT aspiration was dose dependent and observed in both heart and liver homogenates (15–34% increase over control) but not in the lungs.

Biomarkers of oxidative stress in the BAL fluids and tissues

Oxidative damage after exposure to SWCNTs was evaluated by the presence of HNE–His adducts (lipid peroxidation end product) (Fig. 3C). SWCNT exposure caused an increase of up to ninefold vs the control in the HNE–His adduct level in the BAL of the exposed mice on day 1 after pharyngeal aspiration.

The level of oxidative injury in the lungs, heart, and liver caused by SWCNTs on day 7 post-pharyngeal aspiration was assessed by GSH, protein thiols, the lipid peroxidation end product HNE–His adduct, and oxidatively modified proteins measured as protein carbonyls (Fig. 5). At 7 days postexposure, we found no significant changes in the biomarkers of oxidative stress in the lung homogenates, but the level of oxidative damage in the heart and liver was significantly different from that of the control group. Dose-dependent GSH depletion in the heart or liver of mice exposed to 40 and 80 μg/mouse represented a significant (6 and 11%, 7 and 19%, respectively) decrease from control (Fig. 5A). Changes in the levels of protein thiols in the mouse heart after aspiration of 40 or 80 μg/mouse of SWCNTs revealed a significant 7 or 10% decrease, respectively, from the control (Fig. 5B), whereas in

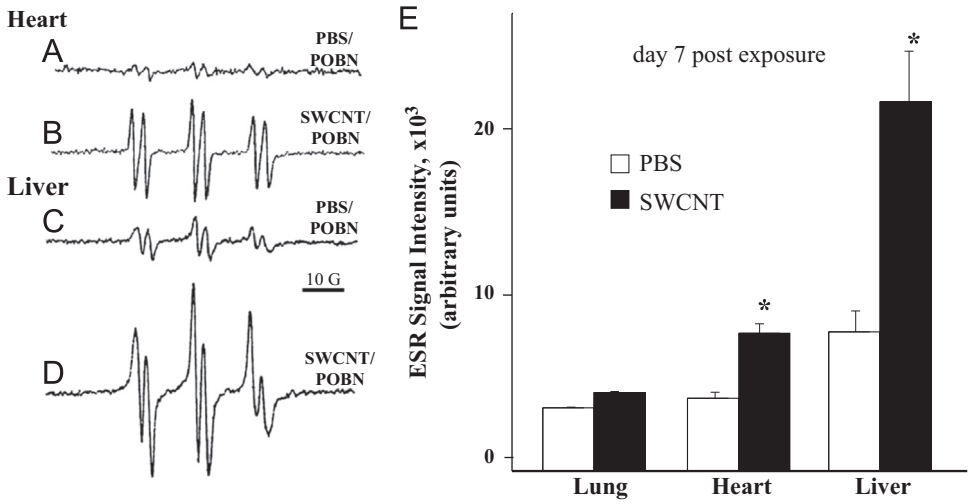

Fig. 2. Free radical generation by SWCNTs in lipid extracts of lungs, heart, and liver 7 days after treatment. (A–D) Representative ESR spectra of POBN radical adducts detected in (B) heart and (D) liver of mice 30 min after injection of the spin trap POBN (6 mmol/kg, ip) on day 7 post-SWCNT exposure. (A) Same as for (B) but mice were treated with PBS. (C) Same as for (D) but mice were treated with PBS. (E) Results of relative values of ESR signal intensity (arbitrary units) represent the mean ± SE derived from four or five independent experiments. $^{*}p < 0.05$, significantly different from controls.

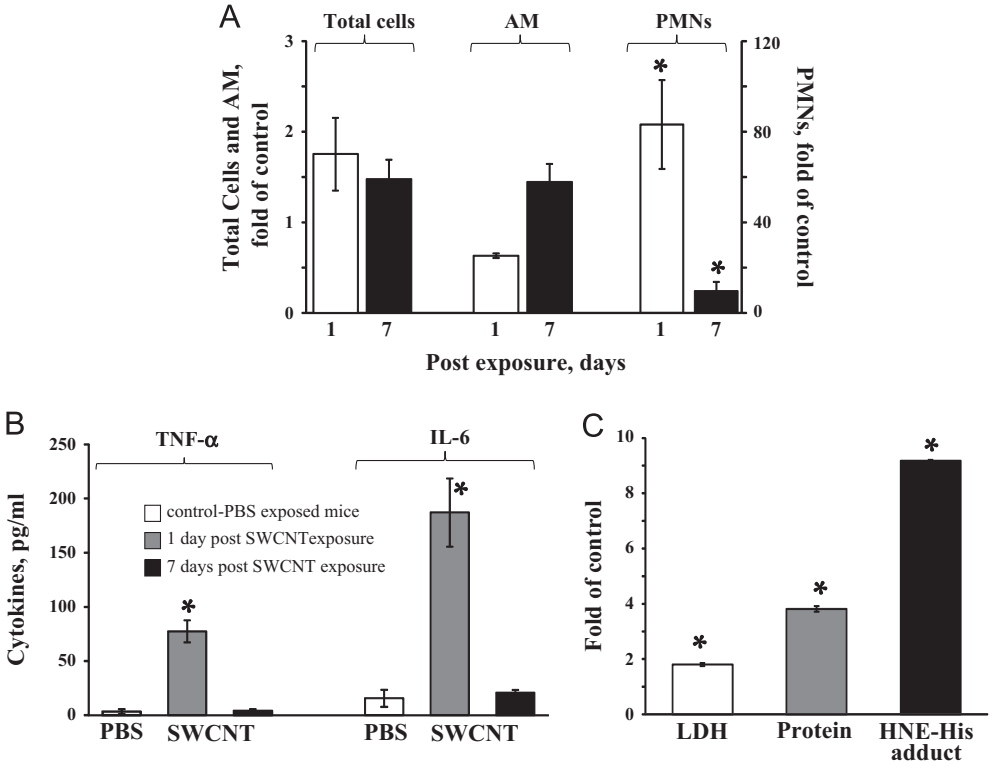

Fig. 3. (A) Cell profile of bronchoalveolar lavage samples from mice after pharyngeal aspiration with SWCNTs: Open columns, 1 day after exposure to SWCNTs (40 μg/mouse); black columns, 7 days after exposure to SWCNTs (40 μg/mouse). $^{*}p < 0.05$, significantly different from controls. (B) Accumulation of proinflammatory cytokines in the BAL fluid of mice after aspiration of 40 μg/mouse SWCNTs evaluated by changes in the level of TNF-α and IL-1β. $^{*}p < 0.05$, significantly different from controls. (C) Pulmonary damage after aspiration of 40 μg/mouse SWCNTs, evaluated by changes in the levels of LDH and protein, and the degree of lipid peroxidation assessed by HNE–His adduct in the BAL fluid of mice on day 1 after exposure. Data are expressed as fold increase vs controls exposed to PBS. $^{*}p < 0.05$, significantly different from controls.

the liver we detected a 50% depletion of protein thiols. The level of lipid peroxidation products measured as HNE–His adduct showed no significant dose-dependent increase in the lung homogenates on day 7 after exposure to SWCNTs. However, significant dose-dependent (11 and 20%) accumulation of HNE–His adducts was detected in the heart homogenate, whereas in the liver we found a 40% increase over the control (Fig. 5C). A significant dose-dependent elevation of the levels of protein carbonyls (24 and 44%) was observed in the heart after exposure to SWCNTs at 7 days posttreatment (40 and 80 μg/mouse, respectively), whereas in the liver, the level of protein carbonyls increased significantly (20%) for both concentrations of SWCNTs (Fig. 5D).

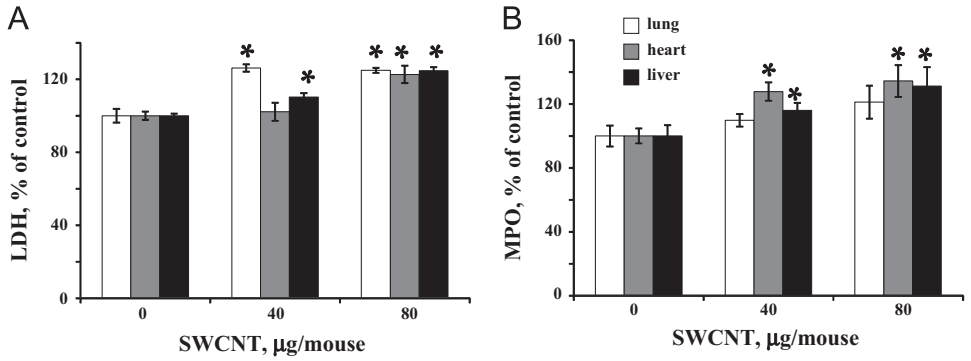

Fig. 4. Tissue damage and inflammation evaluated by the changes in the levels of (A) LDH and (B) MPO activity in the lungs, heart, and liver 7 days after pharyngeal aspiration of SWCNTs (40 and 80 μg/mouse). Data are expressed as % of controls exposed to PBS. *$p < 0.05$, significantly different from controls.

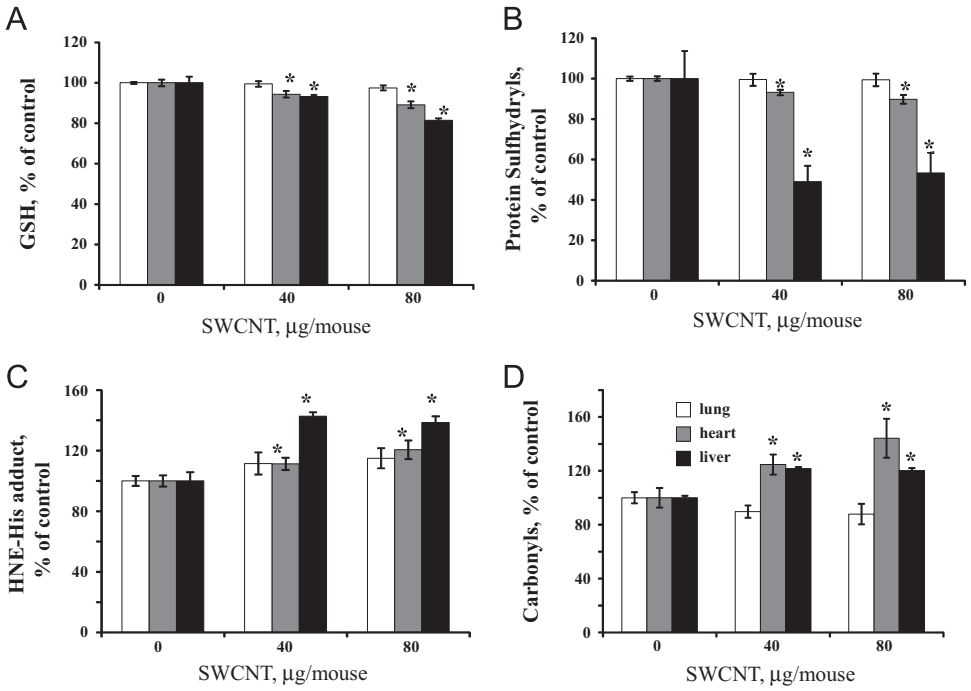

Fig. 5. The degree of oxidative stress evaluated by (A) GSH, (B) protein sulfhydryls, (C) HNE–His adduct, and (D) protein carbonyls in the lungs, heart, and liver of mice on day 7 after exposure to 40 or 80 μg/mouse SWCNTs. Data are expressed as % of controls exposed to PBS. *$p < 0.05$, significantly different from controls.

Effect of deferoxamine on the lung inflammation and oxidative stress induced by SWCNTs

To determine whether iron-dependent species were involved in the induction of inflammation or oxidative stress in the lungs of mice 24 h after exposure to SWCNTs, we used the iron chelator desferoxamine. When mice were pretreated with DFO 2 and 24 h before pharyngeal aspiration with SWCNTs, the production of inflammatory cytokines IL-1α, IL-6, IFN-γ, and TNF-α was significantly inhibited by 46, 50, 60, and 50%, respectively (Fig. 6A). Additionally, the level of MPO activity, a biomarker of tissue inflammation, measured in the lung homogenates 24 h after exposure to SWCNTs was significantly reduced by 39% (Fig. 6B). Moreover, preexposure of mice to DFO significantly increased the level of a major antioxidant, glutathione, by 55% and decreased the concentration of HNE–His adducts by 24% (Fig. 6C).

Characterization of fibrogenic response

Morphologic findings are consistent with the rapid development of granulomatous bronchointerstitial pneumonia after pharyngeal aspiration of 40 μg/mouse SWCNTs (Fig. 7). The material persisted in the lungs throughout the study period and remained localized near the terminal bronchioles and alveolar ducts. The inflammation evolved with time from principally neutrophilic to principally granulomatous. Well-formed granulomas were a component of the granulomatous response. These granulomas were space-occupying and sometimes compressed or extended into the lumen of bronchioles. At 1 day after exposure, nanotubes were principally extracellular and localized to the lumen and luminal surface of terminal bronchioles and alveolar ducts (Fig. 7B).

The inflammatory response was rapid and at 1 day after exposure was composed principally of neutrophils with a variable histiocytic response. The distribution of the inflammatory response was multifocal and the severity ranged from mild to moderate. At 7 days postexposure, the inflammation was granulomatous or pyogranulomatous (Fig. 7D). Well-formed multifocal, moderate pyogranulomas were present and were principally distributed in the interstitium of bronchiolar walls, alveolar ducts, and adjacent alveoli. Macrophages and granulomas frequently extend into and obscure the lumen of terminal bronchioles. The

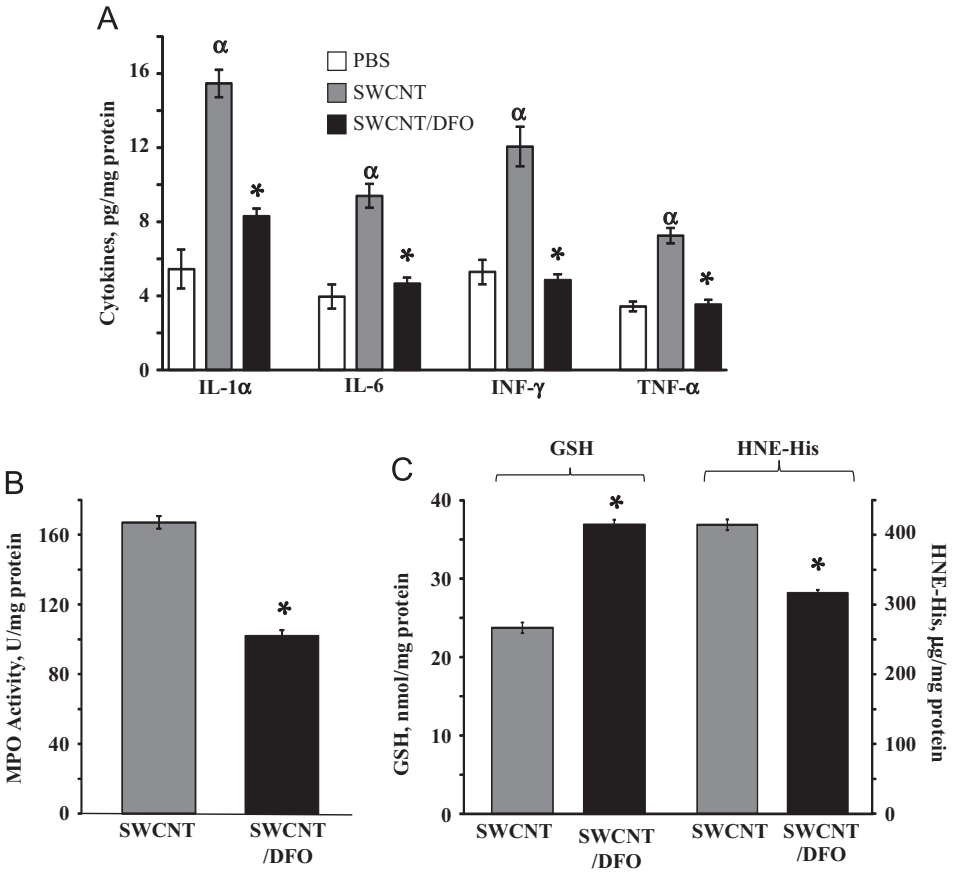

Fig. 6. Effect of deferoxamine on inflammation and oxidative stress induced by SWCNTs. Mice were pretreated with deferoxamine (DFO; 100 mg/kg, ip) 2 and 24 h before pharyngeal aspiration of SWCNTs (40 μg/mouse). (A) Accumulation of proinflammatory cytokines in the lung homogenates on day 1 after pharyngeal aspiration of 40 μg/mouse SWCNTs was evaluated by changes in the levels of IL-1α, IL-6, IFN-γ, and TNF-α. $^{\alpha}p < 0.001$, significantly different from controls. $^{*}p < 0.001$, significantly different from SWCNTs alone exposure group. (B) MPO activity in the lung homogenates on day 1 after pharyngeal aspiration of 40 μg/mouse SWCNTs. $^{*}p < 0.001$, significantly different from SWCNTs alone exposure group. (C) Oxidative stress assessed by the changes in the levels of GSH and HNE–His adducts in the lung homogenates of mice on day 1 after exposure to 40 μg/mouse SWCNTs. $^{*}p < 0.05$, significantly different from SWCNTs alone exposure group.

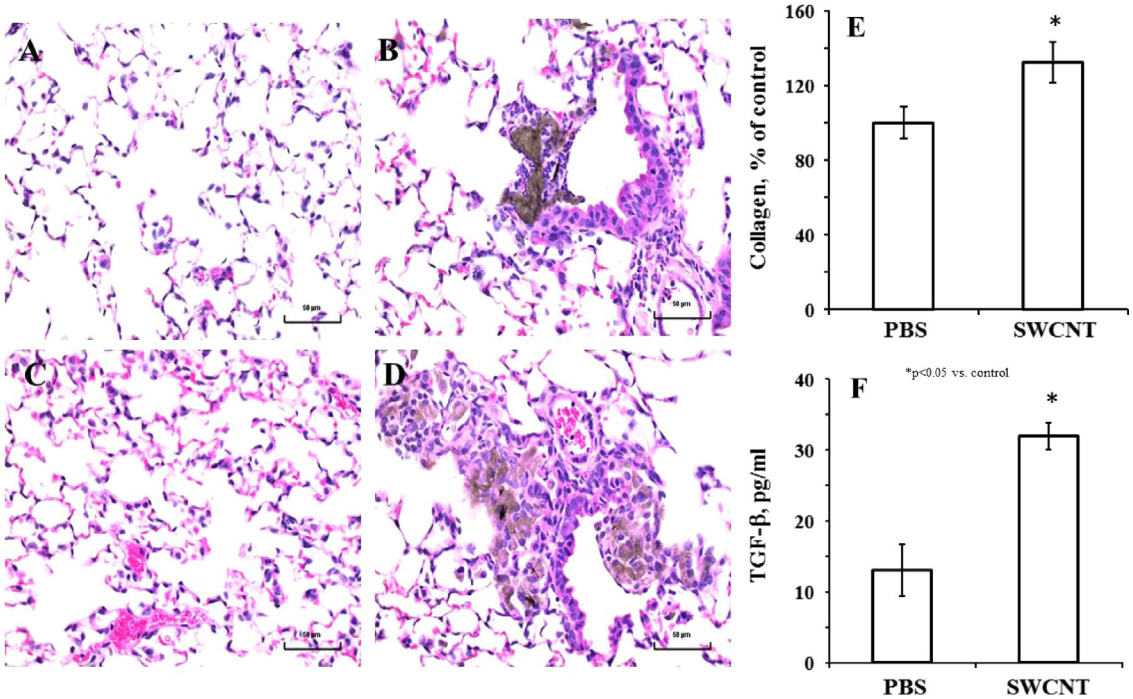

Fig. 7. Light micrographs of H&E-stained sections from lungs of mice 1 and 7 days after pharyngeal aspiration of SWCNT (40 μg/mouse): 1 day after treatment with (A) PBS or (B) SWCNTs; 7 days after treatment with (C) PBS or (D) SWCNTs. Accumulation of (E) collagen in the lung homogenates and (F) TGF-β in the BAL of mice on day 7 after exposure to 40 μg/mouse SWCNTs. $^{*}p < 0.05$, significantly different from controls.

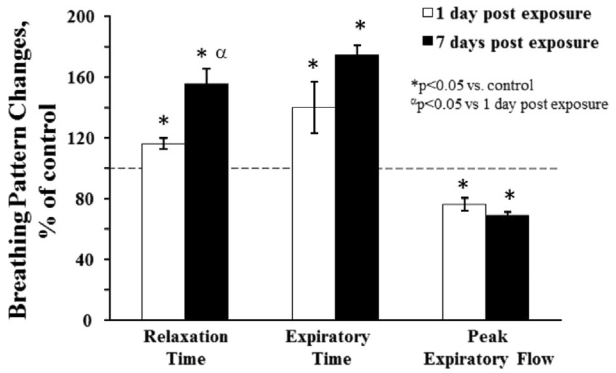

Fig. 8. Changes in breathing pattern after pharyngeal aspiration with SWCNTs (40 μg/mouse). Means ± SEM ($n=6$ mice/group). *$p < 0.05$ vs control PBS-exposed mice, $^{\alpha}p < 0.05$ vs 1 day after exposure to SWCNTs.

green-gray foreign material was generally intracytoplasmic in location as variably sized aggregates.

Collagen deposition and pulmonary fibrosis are typical features of the inflammatory response to various injuries to the lung, including particulate injury. The collagen accumulation in the lungs of C57BL/6 mice after aspiration of SWCNTs revealed a significant (32%) increase over PBS control groups at 7 days postexposure (Fig. 7E). A significant elevation of fibrogenic TGF-β1 release (2.5-fold over control) was also found in the BAL fluid of C57BL/6 mice on day 7 after SWCNT aspiration (Fig. 7B). No significant changes, compared to the control, were found for TGF-β or collagen on day 1 after exposure to SWCNTs (data not shown).

Pulmonary function

Exposure to a lung irritant can lead to changes in breathing patterns. SWCNT pharyngeal aspiration (40 μg/mouse) caused minor changes in pulmonary function. Elevated relaxation time and expiratory times were detected as early as 1 day after exposure to SWCNTs, with a maximum on day 7 (Fig. 8). These changes were accompanied by decreases in the peak expiratory flow, compared to PBS-exposed animals, on day 1 after SWCNT aspiration, and they persisted for 7 days (Fig. 8).

Discussion

Nanomaterials have received substantial attention recently because of their unique properties and applications. Regardless of the rapid progress and early positive recognition of nanotechnology, the potential for adverse health effects in humans and for the environment has not been well known. In this study, oxidative stress and inflammatory responses were examained in mouse lungs, liver, and heart on days 1 and 7 post-pharyngeal aspiration of a bolus dose of SWCNTs (40–80 μg/mouse) to confirm not only damage at the deposition site but also distant responses as a result of particle translocation and/or reactivity throughout the body.

Because free radicals in biological systems are characterized by their high reactivity, short lifetimes, and low concentrations, the type of spin trap used is a key factor in determining how informative and sensitive the spin trapping technique may be for a given radical species. In a number of earlier reported spin trapping studies, the use of the nitrone spin trap POBN was well substantiated. POBN is a well-recognized spin trapping agent that has proven a good tool to record free radicals owing to several intrinsic features, such as good hydrophilicity (solubility), good stability, and relatively low toxicity, all of which are highly essential for in vivo studies in animals [16,38].

We have provided ESR evidence that free radicals are generated in vivo in the lung, heart, and liver after pulmonary exposure to respirable SWCNTs (Figs. 1 and 2). Based on ESR spectral simulations, we identified the radical adducts as carbon-centered and lipid-derived. The carbon-centered radicals detected are conceivably an intermediate of enhanced lipid peroxidation in the lung caused by exposure to respirable SWCNTs in vivo, as was reported previously [38,44–46]. We found that the pharyngeal aspiration of SWCNTs significantly enhanced free radicals in the lung on day 1 postexposure, primarily in the form of lipid-derived carbon-centered free radicals detected as POBN radical adducts in this study (Fig. 1). Further, free radical production was clearly correlated with the recruitment of neutrophils found in BAL fluids recovered from exposed mice (Fig. 3A) together with the accumulation of the proinflammatory cytokines TNF-α and IL-6 (Fig. 3B) and signs of pulmonary damage (Figs. 3C and 4). Additionally, histopathological analysis of the lung tissue at the same time point (1 day post-treatment) revealed a rapid inflammatory response that was composed principally of neutrophils with a variable histocytic response (Fig. 7B). All these findings were followed as indices of lung injury and were assessed to determine whether radical generation preceded or was associated with changes in the lungs. Although SWCNTs did not significantly enhance alveolar macrophage numbers in the bronchoalveolar lavage, they significantly increased neutrophil counts. These data demonstrate that free radical generation was associated with severe lung inflammation as a result of neutrophil infiltration caused by SWCNTs. This is consistent with other studies that showed increased oxidative stress correlated with inflammation [44,45].

Although no direct evidence has been presented for the generation of hydroxyl radicals in our animal model, we provide conclusive evidence that radical adducts are formed from endogenous molecules such as polyunsaturated fatty acids. We suggest that the radical responsible for the POBN adduct is carbon-centered and derived from endogenous lipids as a result of enhanced lipid peroxidation by SWCNTs. This is the most direct ESR evidence yet of lipid peroxidation-associated free radical formation in the toxicity of SWCNTs. Had the generation of hydroxyl radicals been the primary toxic action of SWCNTs in these experiments, then the DMSO-dependent POBN/$^{\bullet}CH_3$ and POBN/$^{\bullet}OCH_3$ should have been detected [40]. From the hyperfine splitting constants obtained for the radical adduct shown in Figs. 1 and 2, and the lack of a carbon-13 isotope splitting when [^{13}C]DMSO was used, it is apparent that the radical adduct is not a hydroxyl radical reacting with DMSO to form a stable 12-line spectrum of POBN/$^{\bullet}CH_3$ and POBN/$^{\bullet}OCH_3$ radical adducts. It should be noted, however, that an inability to detect radical adducts by ESR is not proof that they are not formed in vivo. A number of factors, such as the relative rates of radical adduct formation, destruction, and excretion, can all affect the detection of a radical adduct.

In our study, pretreatment of mice with the iron chelator DFO significantly inhibited biomarkers of inflammation and oxidative stress, including lipid peroxidation in the lung tissue (Fig. 6), which supports the important role of iron in toxicological effects of SWCNTs. Despite not being monitored in this study, we can speculate that pretreatment with DFO could also affect free radical generation in the tissue of mice triggered by SWCNTs based on the shown protective effect of DFO on lung inflammation and lipid peroxidation, as well as information from previously published data [18,38]. There are reports demonstrating that the existence of metal catalytic residues can initiate/aggravate the adverse effects induced by CNTs [29,47–49]. The enhancement of oxidative stress by iron-containing SWCNTs can change the normal course of

macrophage-dependent development of the inflammatory response. The key toxicity of nanoparticles has been attributed to their unique physicochemical characteristics—small size, large surface area, and high surface reactivity [50]. This physicochemical reactivity is frequently correlated with the ability of nanoparticles to trigger the formation of free radicals directly or via activation of oxidative enzymatic pathways, leading to oxidative stress. The major sources of oxidative stress are transition metal-based nanoparticles or transition metal contaminants used as catalysts during production of nonmetal nanoparticles, including SWCNTs and relatively stable free radical intermediates present on "reactive" surfaces of particles such as carbonaceous nanomaterials [9]. Kagan and colleagues [47] showed that the iron content of SWCNTs was important for enhanced catalysis of extracellular oxidative stress as well as for intracellular depletion of antioxidants (ascorbate and GSH) and accumulation of lipid peroxidation products in macrophages. In this study, we used HiPco materials that were produced utilizing iron as the catalytic metal. SWCNTs were partially purified by acid treatment to remove metal contaminants [34]. As a result, the iron content of the SWCNTs was dramatically reduced but still remained at the level of 0.23 wt%. Even the smallest iron contamination imparts radical reactivity, hence toxicity [51].

Although the initial increase in the ESR signal observed in the lung on day 1 posttreatment was triggered as a first line of cellular defense against direct pulmonary exposure, investigation of the systemic changes in other organs (heart and liver) at the later time point was essential. We found a significant increase in the intensity of ESR radicals only in the heart and liver of mice on day 7 post-SWCNT exposure (Fig. 2), not in the lungs. These alterations in the heart and liver were accompanied by increased inflammation (MPO; Fig. 4) and increased levels of oxidative stress markers, including depletion of antioxidants, accumulation of lipid peroxidation products, and modified proteins (Fig. 5). Our previously published results indicate that, contrary to the well-established chain of events, nonfunctionalized SWCNTs are not particularly well recognized by macrophages and hence are not active as targets of macrophage engulfment and phagocytosis [44]. Therefore, the failure of macrophages to recognize dispersed SWCNTs in vivo may result in their translocation into the systemic circulation, distribution, and subsequent effects on distant tissues including cardiovascular damage and liver and brain injury.

These distant translocations/effects of nanoparticles, including SWCNTs and MWCNTs, have been reported previously [24–31,52–54]. Stapleton and colleagues [28] reported that inhaled MWCNT particles elicit inflammatory reactions in the lungs and proinflammatory mediators pass into systemic circulation, contributing to microvascular dysfunction. CNTs can translocate at a very low rate out of the lungs and be visualized within other organ systems (liver, kidney, and heart) 24 h after inhalation exposure. At a lung burden as low as 13.2 μg/lung, the number of inhaled MWCNT fibers was 4535 (0.0007% lung burden) in the liver and 525 (0.00008% of lung burden) in the heart [28]. Mercer et al. [31] reported that at a lung burden of 13.5 μg/lung, MWCNT concentration (fibers per gram of tissue) was 25,767 (0.00281% of lung burden) in the liver and 11,849 (0.00022% of lung burden) in the heart on day 1 post-inhalation exposure; however, by day 336, the level of MWCNT fibers was increased approximately five- to ninefold. Matthews and colleagues [32] predicted that, more than 14 days after exposure, an approximate cumulative pulmonary translocation of SWCNTs from the rat lung will be about 0.15% of a 100-μg deposited dose. The significance of these levels of transport could be critical for health risk assessment. In our study, using a lung burden of 40 μg/mouse, we can suggest that the amount of nanoparticles translocated to the liver will be up to 1.12 ng and to the heart 0.09 ng on day 1 postexposure, with a cumulative translocation of SWCNTs from the lung of about 60 ng. The level of efflux of CNTs from the lung will be similar by day 7 post-exposure [32].

Several toxicological studies have demonstrated that pulmonary exposure to SWCNTs causes a persistent accumulation of carbon nanoparticle aggregates in the lung, followed by the rapid formation of pulmonary granulomatous and fibrotic tissues [44,45]. Accordingly, our morphologic findings from the lung on day 7 postexposure are consistent with the rapid development of granulomatous bronchointerstitial pneumonia (Fig. 7D). Importantly, levels of collagen in the lung and the profibrotic cytokine TGF-β in the BAL of mice on day 7 postexposure to SWCNTs were also significantly elevated. Inflammation and fibrosis in the lung can lead to a damaging decline in pulmonary functions [44,45]. Hence, we asked whether SWCNT exposure caused changes in the breathing pattern. An elevated relaxation time was detected in C57BL6 mice after pharyngeal aspiration to SWCNTs. This alteration was accompanied by an increase in expiratory time and a decrease in the peak expiratory flow as early as day 1 after exposure to SWCNTs (Fig. 8). Changes in expiratory time have been correlated with increased pulmonary resistance in mice [55], and a decline in peak expiratory flow has been found to signify that airways are constricted and could be attributed to asthma [56]. A pronounced increase in the relaxation time could indicate cardiac dysfunction in response to pulmonary toxicity [57]. It has been reported that pulmonary exposure to SWCNTs is associated with an increase in oxidative vascular damage and has the potential to influence cardiovascular diseases [27]. Depletion of GSH and increased protein carbonyls in aortic tissue were also demonstrated and in line with our results. Pulmonary exposure to SWCNTs may induce cardiovascular effects either directly, by translocation of particles to the systemic circulation, or indirectly through mitochondrial oxidative perturbations, which can result in altered vessel homeostasis [27].

Conclusions

Pulmonary exposure to respirable SWCNTs resulted in a rapid augmentation of biomarkers of inflammation and oxidative stress as evidenced by ESR detection of POBN spin-trapped carbon-centered lipid-derived radicals recorded shortly after treatment in the lungs. These alterations were accompanied by recruitment of inflammatory cells, an increase in proinflammatory cytokines, suppressed pulmonary function, and development of interstitial fibrosis. Additionally, pharyngeal aspiration of SWCNTs caused the formation of carbon-centered lipid-derived radicals in the heart and liver at later time points (day 7 postexposure). Moreover, these modifications in the heart and liver were supplemented by increased inflammation (MPO) and elevated levels of oxidative stress markers, including depletion of antioxidants (GSH), accumulation of lipid peroxidation products (HNE–His adducts), and modified proteins (carbonyls). Furthermore, the iron chelator deferoxamine noticeably reduced lung inflammation and oxidative stress, indicating the important role of metal-catalyzed species in lung injury caused by SWCNTs. Overall, respiratory exposure to SWCNTs triggered interactions of early inflammatory response and oxidative stress, culminated in the development of multifocal granulomatous pneumonia and robust interstitial fibrosis, and demonstrated a critical contribution of lipid-derived free radicals to tissue injury.

Acknowledgments

This work was supported by NIOSH OH008282, NORA 92700Y, and NIH RO1 HL-070755. The findings and conclusions in this

report are those of the authors and do not necessarily represent the views of the National Institute for Occupational Safety and Health. Part of the research was supported by the Intramural Program of the NIH, National Institute of Environmental Health Sciences.

References

[1] Dillon, A. C.; Nelson, B. P.; Zhao, Y.; Kim, Y. -H.; Tracy, C. E.; Zhang, S. B. Importance of turning to renewable energy resources with hydrogen as a promising candidate and on-board storage a critical barrier. *Mater. Res. Soc. Symp. Proc* 895; 2006.

[2] Dillon, A. C. Carbon nanotubes for photoconversion and electrical energy storage. *Chem. Rev.* **110:**6856–6872; 2010.

[3] Endo, M.; Strano, M. S.; Ajayan, P. M. Potential applications of carbon nanotubes. In: Jorio, A., Dresselhaus, G., Dresselhaus, M. S., editors. *Topics in Applied Physics*, Vol. 111. Berlin/Heidelberg: Springer-Verlag; 2008. p. 13–61. (Carbon Nanotubes).

[4] Dai, L.; Chang, D. W.; Baek, J. B.; Lu, W. Carbon nanomaterials for advanced energy conversion and storage. *Small* **8:**1130–1166; 2012.

[5] Dahlben, L. J.; Eckelman, M. J.; Hakimian, A.; Somu, S.; Isaacs, J. Environmental life cycle assessment of a carbon nanotube-enabled semiconductor device. *Environ. Sci. Technol.* **47:**8471–8478; 2013.

[6] G.X. Wang, J.H. Ahn, J. Yao, M. Lindsay, H.K. Liu, S.X. Dou (2003) Preparation and characterization of carbon nanotubes for energy storage. J Power Sources **119**(121), 2003, 16–23.

[7] Beaudrie, C. E.; Kandlikar, M.; Satterfield, T. From cradle-to-grave at the nanoscale: gaps in U.S. regulatory oversight along the nanomaterial life cycle. *Environ. Sci. Technol.* **47:**5524–5534; 2013.

[8] Shvedova, A. A.; Kisin, E. R.; Murray, A. R.; Kommineni, C.; Castranova, V.; Mason, R. P.; Kadiiska, M. B.; Gunther, M. R. Antioxidant balance and free radical generation in vitamin E-deficient mice after dermal exposure to cumene hydroperoxide. *Chem. Res. Toxicol.* **15:**1451–1459; 2002.

[9] Shvedova, A. A.; Pietroiusti, A.; Fadeel, B.; Kagan, V. E. Mechanisms of carbon nanotube-induced toxicity: focus on oxidative stress. *Toxicol. Appl. Pharmacol.* **261:**121–133; 2012.

[10] Shvedova A.A., Kisin E.R., Murray A.R., Schwegler-Berry D., Gandelsman V.Z., Baron P., Maynard A., Gunther M.R., Castranova V. Exposure of human bronchial epithelial cells to carbon nanotubes causes oxidative stress and cytotoxicity. In: Proceedings of the Society for Free Radical Research Meeting, European Section, Ioannina, Greece; 26–29 June 2003; pp. 91–103.

[11] Kagan, V. E.; Bayir, H.; Shvedova, A. A. Nanomedicine and nanotoxicology: two sides of the same coin. *Nanomedicine* **1:**313–316; 2005.

[12] Pulskamp, K.; Diabaté, S.; Krug, H. F. Carbon nanotubes show no sign of acute toxicity but induce intracellular reactive oxygen species in dependence on contaminants. *Toxicol. Lett.* **168:**58–74; 2007.

[13] Wardman, P. Fluorescent and luminescent probes for measurement of oxidative and nitrosative species in cells and tissues: progress, pitfalls, and prospects. *Free Radic. Biol. Med.* **43:**995–1022; 2007.

[14] Bonini, M. G.; Rota, C.; Tomasi, A.; Mason, R. P. The oxidation of 2′,7′-dichlorofluorescein to reactive oxygen species: a self-fulfilling prophesy? *Free Radic. Biol. Med* **40:**968–975; 2006.

[15] Kalyanaraman, B.; Darley-Usmar, V.; Davies, K. J.; Dennery, P. A.; Forman, H. J.; Grisham, M. B.; Mann, G. E.; Moore, K.; Roberts 2nd L. J.; Ischiropoulos, H. Measuring reactive oxygen and nitrogen species with fluorescent probes: challenges and limitations. *Free Radic. Biol. Med.* **52:**1–6; 2012.

[16] Mason, R. P. *in vivo* spin-trapping—from chemistry to toxicology. In: Rhodes, C. J., editor. *Toxicology of the Human Environment: the Critical Role of Free Radicals*. London: Taylor & Francis; 2000. p. 49–70.

[17] Winterbourn, C. C. Reconciling the chemistry and biology of reactive oxygen species. *Nat. Chem. Biol.* **4:**278–286; 2008.

[18] Dikalova, A. E.; Kadiiska, M. B.; Mason, R. P. An in vivo ESR spin-trapping study: free radical generation in rats from formate intoxication—role of the Fenton reaction. *Proc. Natl. Acad. Sci. USA* **98:**13549–23553; 2001.

[19] Kadiiska, M. B.; Morrow, J. D.; Awad, J. A.; Roberts 2nd L. J.; Mason, R. P. Identification of free radical formation and F2-isoprostanes in vivo by acute Cr (VI) poisoning. *Chem. Res. Toxicol.* **11:**1516–1520; 1998.

[20] Kadiiska, M. B.; Mason, R. P. Acute methanol intoxication generates free radicals in rats: an ESR spin trapping investigation. *Free Radic. Biol. Med.* **28:**1106–1114; 2000.

[21] Kadiiska, M. B.; Mason, R. P.; Dreher, K. L.; Costa, D. L.; Ghio, A. J. in vivo evidence of free radical formation in the rat lung after exposure to an emission source air pollution particle. *Chem. Res. Toxicol.* **10:**1104–1108; 1997.

[22] Kadiiska, M. B.; Ghio, A. J.; Mason, R. P. ESR investigation of the oxidative damage in lungs caused by asbestos and air pollution particles. *Spectrochim. Acta A Mol. Biomol. Spectrosc* **60:**1371–1377; 2004.

[23] Kreyling, W. G.; Semmler-Behnke, M.; Seitz, J.; Scymczak, W.; Wenk, A.; Mayer, P.; Takenaka, S.; Oberdorster, G. Size dependence of the translocation of inhaled iridium and carbon nanoparticle aggregates from the lung of rats to the blood and secondary target organs. *Inhalation Toxicol* **21(Suppl. 1):**55–60; 2009.

[24] Reddy, A. R.; Rao, M. V.; Krishna, D. R.; Himabindu, V.; Reddy, Y. N. Evaluation of oxidative stress and anti-oxidant status in rat serum following exposure of carbon nanotubes. *Regul. Toxicol. Pharmacol.* **59:**251–257; 2011.

[25] Reddy, A. R.; Krishna, D. R.; Reddy, Y. N.; Himabindu, V. Translocation and extra pulmonary toxicities of multi wall carbon nanotubes in rats. *Toxicol. Mech. Methods* **20:**267–272; 2010.

[26] Khandoga, A.; Stoeger, T.; Khandoga, A. G.; Bihari, P.; Karg, E.; Ettehadieh, D.; Lakatos, S.; Fent, J.; Schulz, H.; Krombach, F. Platelet adhesion and fibrinogen deposition in murine microvessels upon inhalation of nanosized carbon particles. *J. Thromb. Haemostasis* **8:**1632–1640; 2010.

[27] Li, Z.; Hulderman, T.; Salmen, R.; Chapman, R.; Leonard, S. S.; Young, S. H.; Shvedova, A.; Luster, M. I.; Simeonova, P. P. Cardiovascular effects of pulmonary exposure to single-wall carbon nanotubes. *Environ. Health Perspect.* **115:**377–382; 2007.

[28] Stapleton, P. A.; Minarchick, V. C.; Cumpston, A. M.; McKinney, W.; Chen, B. T.; Sager, T. M.; Frazer, D. G.; Mercer, R. R.; Scabilloni, J.; Andrew, M. E.; Castranova, V.; Nurkiewicz, T. R. Impairment of coronary arteriolar endothelium-dependent dilation after multi-walled carbon nanotube inhalation: a time-course study. *Int. J. Mol. Sci* **13:**13781–13803; 2012.

[29] Ge, C.; Meng, L.; Xu, L.; Bai, R.; Du, J.; Zhang, L.; Li, Y.; Chang, Y.; Zhao, Y.; Chen, C. Acute pulmonary and moderate cardiovascular responses of spontaneously hypertensive rats after exposure to single-wall carbon nanotubes. *Nanotoxicology* **6:**526–542; 2012.

[30] Legramante, J. M.; Valentini, F.; Magrini, A.; Palleschi, G.; Sacco, S.; Iavicoli, I.; Pallante, M.; Moscone, D.; Galante, A.; Bergamaschi, E.; Bergamaschi, A.; Pietroiusti, A. Cardiac autonomic regulation after lung exposure to carbon nanotubes. *Hum. Exp. Toxicol.* **28:**369–375; 2009.

[31] Mercer, R. R.; Scabilloni, J. F.; Hubbs, A. F.; Wang, L.; Batteli, L. A.; McKinney, W.; Castranova, V.; Porter, D. W. Extrapulmonary transport of MWCNT following inhalation exposure. *Part. Fibre Toxicol* **10:**38; 2013.

[32] Matthews, I. P.; Gregory, C. J.; Aljayyoussi, G.; Morris, C. J.; McDonald, I.; Hoogendoorn, B.; Gumbleton, M. Maximal extent of translocation of single-walled carbon nanotubes from lung airways of the rat. *Environ. Toxicol. Pharmacol.* **35:**461–464; 2013.

[33] Scott, C. D.; Povitsky, A.; Dateo, C.; Gokcen, T.; Willis, P. A.; Smalley, R. E. Iron catalyst chemistry in modeling a high-pressure carbon monoxide nanotube reactor. *J. Nanosci. Nanotechnol.* **3:**63–73; 2003.

[34] Gorelik, O.; Nikolaev, P.; Arepalli, S. *Purification Procedures for Single-Walled Carbon Nanotubes. NASA Contractor Report (NASA/CR-2000-208926)*. Hanover, MD: NASA; 2000.

[35] Knecht, K. T.; Mason, R. P. in vivo spin trapping of xenobiotic free radical metabolites. *Arch. Biochem. Biophys.* **303:**185–194; 1993.

[36] Ghio, A. J.; Kadiiska, M. B.; Xiang, Q. H.; Mason, R. P. in vivo evidence of free radical formation after asbestos instillation: an ESR spin trapping investigation. *Free Radic. Biol. Med.* **24:**11–17; 1998.

[37] Duling, D. R. Simulation of multiple isotropic spin-trap EPR spectra. *J. Magn. Reson. B* **104:**105–110; 1994.

[38] Sato, K.; Corbett, J.; Mason, R. P.; Kadiiska, M. B. in vivo evidence of free radical generation in the mouse lung after exposure to Pseudomonas aeruginosa bacterium: an ESR spin-trapping investigation. *Free Radic. Res.* **46:**645–655; 2012.

[39] Kadiiska, M. B.; Mason, R. P. Ethylene glycol generates free radical metabolites in rats: an ESR in vivo spin trapping investigation. *Chem. Res. Toxicol.* **13:**1187–1191; 2000.

[40] Yue Qian, S.; Kadiiska, M. B.; Guo, Q.; Mason, R. P. A novel protocol to identify and quantify all spin trapped free radicals from in vitro/in vivo interaction of $HO^{\bullet}$ and DMSO: LC/ESR, LC/MS, and dual spin trapping combinations. *Free Radic. Biol. Med.* **38:**125–135; 2005.

[41] Nakai, K.; Kadiiska, M. B.; Jiang, J. J.; Stadler, K.; Mason, R. P. Free radical production requires both inducible nitric oxide synthase and xanthine oxidase in LPS-treated skin. *Proc. Natl. Acad. Sci. USA* **103:**4617–4621; 2006.

[42] Miyakawa, H.; Mason, R. P.; Jiang, J.; Kadiiska, M. B. Lipid-derived free radical production in superantigen-induced interstitial pneumonia. *Free Radic. Biol. Med.* **47:**241–249; 2009.

[43] Burkitt, M. J.; Mason, R. P. Direct evidence for in vivo hydroxyl-radical generation in experimental iron overload: an ESR spin-trapping investigation. *Proc. Natl. Acad. Sci. USA* **88:**8440–8444; 1991.

[44] Shvedova, A. A.; Kisin, E. R.; Mercer, R.; Murray, A. R.; Johnson, V. J.; Potapovich, A. I.; Tyurina, Y. Y.; Gorelik, O.; Arepalli, S.; Schwegler-Berry, D.; Hubbs, A. F.; Antonini, J.; Evans, D. E.; Ku, B. K.; Ramsey, D.; Maynard, A.; Kagan, V. E.; Castranova, V.; Baron, P. Unusual inflammatory and fibrogenic pulmonary responses to single-walled carbon nanotubes in mice. *Am. J. Physiol. Lung Cell Mol. Physiol* **289:**L698–708; 2005.

[45] Shvedova, A. A.; Kisin, E.; Murray, A. R.; Johnson, V. J.; Gorelik, O.; Arepalli, S.; Hubbs, A. F.; Mercer, R. R.; Keohavong, P.; Sussman, N.; Jin, J.; Yin, J.; Stone, S.; Chen, B. T.; Deye, G.; Maynard, A.; Castranova, V.; Baron, P. A.; Kagan, V. E. Inhalation vs. aspiration of single-walled carbon nanotubes in C57BL/6 mice: inflammation, fibrosis, oxidative stress, and mutagenesis. *Am. J. Physiol. Lung Cell Mol. Physiol* **295:**L552–565; 2008.

[46] Sato, K.; Kadiiska, M. B.; Ghio, A. J.; Corbett, J.; Fann, Y. C.; Holland, S. M.; Thurman, R. G.; Mason, R. P. in vivo lipid-derived free radical formation by NADPH oxidase in acute lung injury induced by lipopolysaccharide: a model for ARDS. *FASEB J* **16:**1713–1720; 2002.

[47] Kagan, V. E.; Tyurina, Y. Y.; Tyurin, V. A.; Konduru, N. V.; Potapovich, A. I.; Osipov, A. N.; Kisin, E. R.; Schwegler-Berry, D.; Mercer, R.; Castranova, V.;

Shvedova, P. Direct and indirect effects of single walled carbon nanotubes on RAW 264.7 macrophages: role of iron. *Toxicol. Lett.* **165:**88–100; 2006.

[48] Murray, A. R.; Kisin, E.; Leonard, S. S.; Young, S. H.; Kommineni, C.; Kagan, V. E.; Castranova, V.; Shvedova, A. A. Oxidative stress and inflammatory response in dermal toxicity of single-walled carbon nanotubes. *Toxicology* **257:**161–171; 2009.

[49] Fubini, B.; Fenoglio, I.; Tomatis, M.; Turci, F. Effect of chemical composition and state of the surface on the toxic response to high aspect ratio nanomaterials. *Nanomedicine (London)* **6:**899–920; 2011.

[50] Auffan, M.; Rose, J.; Bottero, J. Y.; Lowry, G. V.; Jolivet, J. P.; Wiesner, M. R. Towards a definition of inorganic nanoparticles from an environmental, health and safety perspective. *Nat. Nanotechnol* **4:**634–641; 2009.

[51] Turci, F.; Tomatis, M.; Lesci, I. G.; Roveri, N.; Fubini, B. The iron-related molecular toxicity mechanism of synthetic asbestos nanofibres: a model study for high-aspect-ratio nanoparticles. *Chemistry* **17:**350–358; 2011.

[52] Oberdorster, G.; Sharp, Z.; Atudorei, V.; Elder, A.; Gelein, R.; Kreyling, W.; Cox, C. Translocation of inhaled ultrafine particles to the brain. *Inhalation Toxicol* **16:**437–445; 2004.

[53] Oberdorster, G.; Maynard, A.; Donaldson, K.; Castranova, V.; Fitzpatrick, J.; Ausman, K.; Carter, J.; Karn, B.; Kreyling, W.; Lai, D.; Olin, S.; Monteiro-Riviere, N.; Warheit, D.; Yang, H. Principles for characterizing the potential human health effects from exposure to nanomaterials: elements of a screening strategy. ILSI Research Foundation/Risk Science Institute Nanomaterial Toxicity Screening Working Group. *Part. Fibre Toxicol* **2:**8; 2005.

[54] Elgrabli, D.; Floriani, M.; Abella-Gallart, S.; Meunier, L.; Gamez, C.; Delalain, P.; Rogerieux, F.; Boczkowski, J.; Lacroix, G. Biodistribution and clearance of instilled carbon nanotubes in rat lung. *Part. Fibre Toxicol* **5:**20; 2008.

[55] Adler, A.; Cieslewicz, G.; Irvin, C. G. Unrestrained plethysmography is an unreliable measure of airway responsiveness in BALB/c and C57BL/6 mice. *J. Appl. Physiol.* **97:**286–292; 2004.

[56] Chan, M.; Sitaraman, S.; Dosanjh, A. Asthma control test and peak expiratory flow rate: independent pediatric asthma management tools. *J. Asthma* **46:**1042–1044; 2009.

[57] Ghobadi, G.; van der Veen, S.; Bartelds, B.; de Boer, R. A.; Dickinson, M. G.; de Jong, J. R.; Faber, H.; Niemantsverdriet, M.; Brandenburg, S.; Berger, R. M.; Langendijk, J. A.; Coppes, R. P.; van Luijk, P. Physiological interaction of heart and lung in thoracic irradiation. *Int. J. Radiat. Oncol. Biol. Phys.* **84:**e639–e646; 2012.